Atmospheric-Induced Amplitude and Phase Fluctuations at Ka-Band

D. D. Morabito[1]

Atmospheric-loss fluctuations due to both water vapor and liquid water contribute to fluctuations in 32-GHz (Ka-band) signals. During weather characterized by high atmospheric liquid water content and varying wind speeds, there will be significant variations in a spacecraft's received signal strength, which will have an impact on spacecraft telemetry data return. The expected dominant effect of severe weather on received Ka-band signals will be on amplitude fading. However, as long as sufficient margin is available, telemetry data return should be nominal.

Received spacecraft signal phase is less significantly affected by liquid water than by water vapor, even during the most severe weather conditions. In this article, spacecraft signal data at Ka-band acquired during a worst-case weather condition pass were analyzed and compared with spacecraft signal data acquired during nominal weather conditions.

I. Introduction

A previous article [1] documented the results of a series of experiments that was conducted for the purpose of characterizing the effects of short-term atmospheric-induced fluctuations on the system operating noise temperature at 32 GHz (Ka-band) at DSS 13 in Goldstone, California. Total power radiometer (TPR) data were simultaneously acquired at both 8.4-GHz (X-band) and 32-GHz frequencies at 1-s integrations rather than the usual 5-s integrations. The fluctuations in the Ka-band TPR zenith sky temperature data presented in [1] at short time scales were found to be dominated by receiver gain fluctuations during clear-weather conditions and were of significantly larger magnitude due to the wet troposphere during cloudy/rainy weather conditions, usually characterized by high liquid water content and varying wind speeds.

Signal degradation due to weather, principally rain, has been a major concern for Earth-orbiting satellite systems operating at Ka-band. A number of programs—such as the Advanced Communications Technology Satellite (ACTS), which was an experimental satellite developed and operated by NASA and its contractors in the United States [2]—have attempted to quantify the rain-fade problem. ACTS was launched in September 1993, and its demonstration experiments, including propagation, were completed in May 2000 [2]. Ka-band propagation experiments using ACTS included statistical measurements on

[1] Communications Systems and Research Section.

The research described in this publication was carried out by the Jet Propulsion Laboratory, California Institute of Technology, under a contract with the National Aeronautics and Space Administration.

fade depths and fade durations as a function of rain rate at the downlink beacon frequencies of 20.2 GHz and 27.5 GHz [3]. The empirical distribution functions for attenuation (in dB versus percent of the year the attenuation was exceeded) were presented for several ACTS sites at these frequencies [3].

This article builds on the work documented in the previous article [1], which focused on short-term system temperature fluctuations. This article analyzes actual spacecraft Ka-band carrier signal strength and phase data acquired during worst-case and nominal weather passes. The contributions due to liquid water are expected to have a lesser effect on path delay rate (frequency), and their principal effect will be on the received signal strength or signal-to-noise ratio (SNR) of any spacecraft being tracked. The atmospheric-induced fluctuations on received signal strength (SNR) for a single-aperture antenna are expected to be the dominating atmospheric factor affecting telemetry reception (as opposed to atmospheric-induced phase fluctuations).

The atmospheric-induced statistics obtained from TPR data and carrier signal data, acquired during selected passes of the Mars Global Surveyor (MGS) Ka-Band Link Experiment (KaBLE-II) [4], are presented. One pass conducted on July 22–23, 1997 (1997/203-204), at Goldstone is of particular interest since the weather conditions were especially rainy and highly variable. Although these conditions are expected to occur less than 1 percent of the time at Goldstone, they provide an instructive picture of worst-case weather effects on Ka-band received signal amplitude and phase. A set of passes conducted during fair or less severe weather conditions was selected for comparison. These included MGS/KaBLE-II passes 1997/205-206, 1997/122, and 1998/090. A study of how the spacecraft carrier signal data acquired during these passes compared with the 1997/203-204 severe-weather pass will also be presented later. Finally, suggestions for strategy on a spacecraft telemetry data link during such conditions are presented, based on the results of this study.

II. Statistical Models and Theory

The model formulation provided in [1] is re-presented and expanded upon here.

The TPR provides estimates of system operating noise temperature, T_{op}, for two independent frequency bands. The input X-band and Ka-band IF channels are filtered using one of several available filters with bandwidth B and sampled and integrated with period T. The relative system operating noise temperature floor (or thermal noise) for the TPR measurements is effectively given by $(BT)^{-1/2}$.

Given a set of T_{op} measurements, the mean and standard deviation of the measurements can be estimated and compared with the predicted thermal noise contribution or with that of other noise contributions. In order to assess the noise contributions at various time scales, the Allan standard deviation (ASD) of the relative temperature measurements is estimated using the definitions in [5].

The fractional temperature averaged over an interval τ at sample time t_k is given by [1]

$$z_k = \left(\frac{T_{op}(t_k + \tau) - T_{op}(t_k)}{\bar{T}_{op}} \right)_k$$

where $\bar{T}_{op}$ is the average T_{op}, which is used to normalize the relative temperature measurements.

A series of measurements is acquired with $t_{k+1} = t_k + \tau, k = 1, 2, 3, \cdots, N$, with each measurement averaged over the time interval τ. For a set of N samples, each taken over this time interval and repetition period, the ASD of the relative temperature fluctuations is given by [5]

$$\sigma_z(\tau) = \sqrt{\left\langle (z_k - \bar{z}_k)^2 \right\rangle} \tag{1}$$

The fluctuations of the relative temperature measurements in Eq. (1) can be analyzed as a function of the time scale. The atmospheric-dominated fluctuations are expected to affect the received signal SNR through attenuation and thermal noise. To infer the effect of these temperature fluctuations on signal phase (or frequency), we can project the relative temperature fluctuations to relative frequency fluctuations. The resulting predicted ASD of the relative frequency fluctuations can then be compared with the actual ASD measured from the carrier signal frequency residuals. Any differences between the two may provide detail on the relative amount of liquid water and water vapor in the atmosphere, which may affect the received signal.

The fluctuation in received carrier frequency, δf, can be related to the change in path delay over a time interval τ, $R(t+\tau) - (R(t)$, by

$$\delta f = f_0 \left(\frac{R(t+\tau) - R(t)}{c\tau} \right)$$

where c is the speed of light and f_0 is the sky frequency. The path delay can be related to the temperature fluctuation, δT, through a conversion factor, Ψ, relating the amount of path delay for each 1 K of temperature variation. At 31.4 GHz, a value for $\Psi = 1.37$ cm/K was obtained from radiosonde data[2] and applied to the 32-GHz TPR data acquired during these experiments. This conversion factor is valid only for low values of atmospheric noise temperature and is due to water vapor only, not water droplets.

The predicted relative frequency fluctuation is thus related to the relative temperature fluctuation by

$$\frac{\delta f}{f_0} = \Psi \left(\frac{T(t+\tau) - T(t)}{c\tau} \right) = \frac{\Psi \bar{T}_{op}}{c\tau} \left(\frac{\delta T_{op}}{\bar{T}_{op}} \right) \tag{2}$$

The ASD of the relative temperature fluctuations in Eq. (1) can be converted to the predicted ASD of relative frequency fluctuations by multiplying by the factor given in Eq. (2) as follows:

$$\sigma_y(\tau) = \left(\frac{\Psi \bar{T}_{op}}{c\tau} \right) \sigma_z(\tau) \tag{3}$$

This estimate of the frequency ASD predicted from T_{op} variations then can be compared with the ASD measured from signal frequency data. If the two are comparable, then water vapor is expected to be the dominant atmospheric constituent, assuming the atmosphere dominates over other noise sources. If the predicted ASD curve lies significantly above the measured ASD curve, then one can assume that the atmosphere contains a sizeable amount of liquid water.

The movement of clouds, rain cells, or clumps of water vapor through the beam of an antenna of diameter D at a wind speed of v_w will induce fluctuations, whose time scales are of the order D/v_w, into the measured T_{op} or received signal strength. In an attempt to detect this effect, the autocorrelation function of received carrier signal strength can be computed and analyzed. Assuming the fluctuations of the atmosphere have significant energy and dominate over other noise sources at the expected time scales, the measured autocorrelation function from the SNR (amplitude) data can be compared with an exponential model of the form

$$\mathcal{R}(\tau) = \exp \left(\frac{-0.693\tau}{\tau_{\text{HPHW}}} \right) \tag{4}$$

[2] S. Keihm, personal communication, Jet Propulsion Laboratory, Pasadena, California, December 2001.

where τ_{HPHW} is the time delay at the half-power half-width point of the autocorrelation function. The model then can be fit to the measured autocorrelation function (after normalization), and the resulting fit parameter, τ_{HPHW}, then can be compared to d/v_w, where d can represent either antenna diameter or Fresnel-zone size, and v_w is the wind speed. The wind speed is measured using ground sensors during the periods of interest.

III. Experiment Configuration

The experiment configuration for DSS 13, the research and development antenna used to acquire the data, was presented in [1], and detail will be reiterated here as appropriate. DSS 13 is a 34-m-diameter beam-waveguide (BWG) antenna located in the Mojave Desert at the Goldstone Deep Space Communications Complex near Barstow, California. This antenna incorporates a series of mirrors inside beam-waveguide tubes that direct and focus the energy into feed packages located in a subterranean pedestal room, which provides a relatively stable environment for the feed and electronics equipment as there is less susceptibility to weather effects. A dichroic plate allows for simultaneous reception of both X-band and Ka-band frequencies.

A "weather system" samples and records a range of meteorological parameters, including atmospheric pressure, air temperature, relative humidity, wind speed, and wind direction. These measurements can be used to predict atmospheric noise temperature and attenuation based on a surface model. Such predictions are of reasonable accuracy during clear, dry conditions, but become increasingly inaccurate during wetter, more severe weather conditions.

A water vapor radiometer (WVR) was measuring sky temperatures, including a 31.4-GHz frequency channel, on-site at DSS 13 during the MGS KaBLE-II experiments. Although the WVR was not co-aligned with the BWG antenna, these data can be used to validate atmospheric noise temperature effects extracted from the T_{op} measurements.

IV. Summary of TPR Experiment Results

The analysis of a series of experiments performed during the latter half of 2001 at DSS 13 for the purpose of characterizing T_{op} fluctuations on short, ∼1-s time scales at Ka-band was presented in [1] and will be summarized briefly here.

The average values and scatter of the ambient and zenith temperature measurements over their respective acquisition periods were computed as one set of statistical measurements. In addition, the ASD of the relative temperature fluctuations, $\sigma_z(\tau)$, was computed [see Eq. (1)] to characterize the fluctuation energy over time intervals of $\tau = 1, 10, 100$, and 1000 s. These values were compared with estimates of individual contributions of gain instability measured during calibrations, thermal noise, and fluctuations deduced from concurrent weather data or WVR sky brightness temperature data at appropriate time scales.

The average and scatter of the T_{op} measurements and the ASDs of the relative temperature measurements while on ambient load for both X-band and Ka-band were found to be consistent with each other and dominated by system effects, principally receiver gain fluctuations, as expected [1].

The TPR statistics acquired while the antenna was pointed at zenith during clear weather at both X-band and Ka-band were essentially consistent with those while on ambient load, suggesting that the non-atmospheric system effects, such as receiver gain variation, dominated during these conditions [1]. The values and signatures of the temperature ASD curves for zenith cold sky showed no significant increase over those of the ambient-load passes between 1-s and 1000-s time scales.

The zenith cold sky temperature measurement time series for the cloudy/rainy weather passes showed significant fluctuations at both X-band and Ka-band. These fluctuations were well correlated with each other, with the appropriate proportions of Ka-band to X-band being consistent with expectations due to the atmosphere. The signatures of these ASD measurements were more positively sloped with time interval, and their magnitudes were significantly increased over those of the clear-weather zenith sky and ambient-load temperature ASD signatures at both frequency bands.

V. Spacecraft Received Carrier Degradation during Severe Weather

The Mars Global Surveyor Ka-Band Link Experiment (MGS/KaBLE-II) was documented in [4]. The TPR data acquired during the experiment passes were sampled at 5-s intervals. Given that the focus of the current study is to characterize worst-case atmospheric effects on a received spacecraft signal at Ka-band, an especially severe weather pass, 1997/203, from MGS/KaBLE-II was selected for study. The T_{op} data for this pass were initially presented in [4], and their statistics were examined in [1]. As the vast majority of the passes on the MGS/KaBLE-II campaign were conducted under nominal weather conditions, it is emphasized that the conditions during much of the 1997/203 pass exceeded 99 percent weather. That is, the likelihood of occurrence of these severe conditions is expected to be significantly less than 1 percent of the time at Goldstone.

A known problem with ice, which accumulated inside the cracked Ka-band feed horn, resulted in a consistent signal strength degradation of about 4 dB and an additional contribution to T_{op} of about 11 K [4]. The ice problem was fixed within a few days after the pass conducted on 1997/203-204, and the feed horn was replaced shortly thereafter [4]. An analysis of clear-weather passes conducted during the period of the known ice problem verified the consistency and repeatability of the 4-dB degradation and the additional 11-K increase in T_{op}. Given that there is a high degree of correlation and consistency between the independent and simultaneous X-band and Ka-band temperature fluctuations, and that the concurrent WVR data support the general character and magnitude of the Ka-band TPR temperature fluctuations, it is believed that the Ka-band fluctuations are real and not an artifact of the accumulated ice. The presence of ice inside the feed horn during this period thus is not expected to affect the general results.

A. T_{op} Data Analysis

Pass 1997/203-204 was conducted during a thunderstorm. The X-band and Ka-band T_{op} data for this pass are shown in Fig. 1 (also presented in [1] and [4]). The changes in T_{op} due to changing elevation angle were not normalized (to refer the atmosphere to one airmass at zenith), as sizeable temporal fluctuations clearly dominate. During spacecraft rise, the DSS-13 antenna was pointed into a very heavy, dark rain cell above the horizon, where prevalent lightning and thunder presented an ominous portent of worst-case Ka-band conditions.

The corresponding relative temperature ASD curves, for X-band and Ka-band, are shown in Fig. 2. The levels and slope of these ASD curves are consistent with those expected due to severe weather, as reported in [1]. Because the data were sampled at 5-s intervals, the curves only extend down to $\log(\tau) = 0.7$. The extrapolation of the ASD curves down to a 1-s ($\log(\tau) = 0$) time scale approaches ASD values of $\simeq 0.001(\log(\sigma_z(\tau)))$, which is consistent with receiver gain instability as measured during minicals.

Figure 3 displays the estimated atmospheric contribution, T_{atm}, to the T_{op} at both X-band and Ka-band, after removing the elevation angle dependence, and referring the measurements to zenith. Figure 4 displays the ratio of the Ka-band atmospheric temperature relative to the X-band atmospheric temperature contribution. Note that the Ka-band atmospheric temperature contribution exceeds 50 K for a significant duration of the pass, while the peak atmospheric temperature reaches a value as high as 195 K at 22:18 UTC (see Fig. 3).

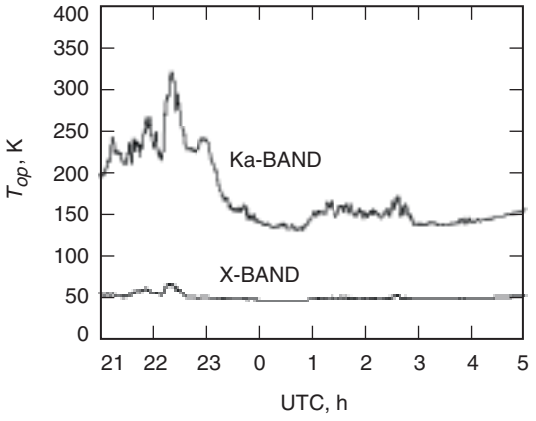

Fig. 1. MGS 1997/203-204 T_{op}.

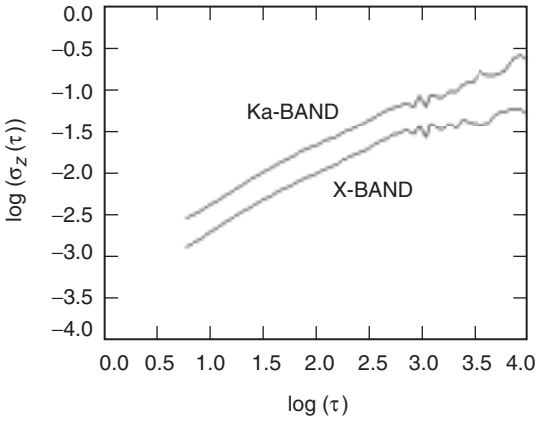

Fig. 2. MGS 1997/203-204 T_{op} Allan deviation.

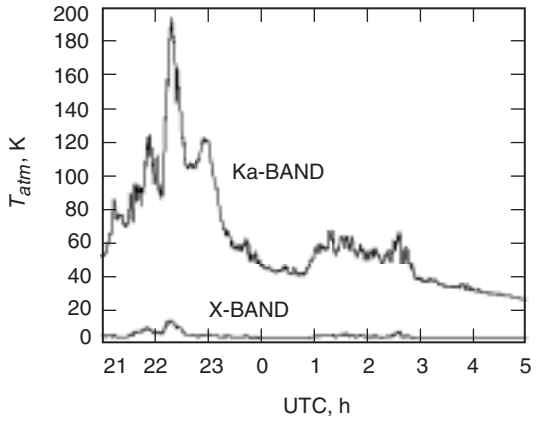

Fig. 3. 1997/203-204 T_{atm} (corrected to zenith).

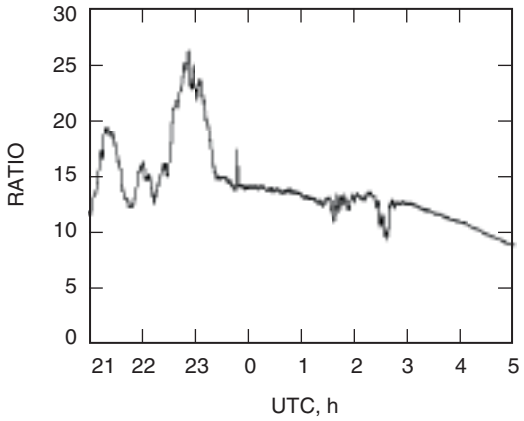

Fig. 4. 1997/203-204 ratio of T_{atm} (Ka)/T_{atm} (X).

Pass 1997/203-204 is characterized by weather, which exceeds 99 percent cumulative distribution. According to [15], this corresponds to a zenith atmospheric contribution of 36 K to the T_{op} at zenith at Goldstone. The atmospheric contribution to the noise temperature exceeded 36 K (referenced at zenith) for much of the pass, as exhibited in the concurrent WVR sky brightness temperature data[3] at 31.4 GHz. The WVR data show the same general features and behavior as the X-band and Ka-band TPR signatures, as was reported in [1].

B. Received Spacecraft Signal Amplitude Data Analysis

The effect of the temperature variations on received spacecraft SNR for 1997/203-204 is now examined. Figure 5 displays the carrier signal power to noise ratio referred to a 1-Hz bandwidth, P_c/N_o, obtained from the Experimental Tone Tracker (ETT) at DSS 13 for each second, for both X-band and Ka-band downlink signals during this severe-weather pass, along with the elevation angle. Both downlink signals were coherent with an X-band signal uplinked from DSS 15, an operational high-efficiency (HEF) 34-m-diameter DSN antenna. To illustrate the effects of weather on received Ka-band carrier signal strength data, refer to Fig. 6, where the data were averaged to remove thermal noise (and scintillation). For reference, the nominal expected clear-weather SNR in a 1-Hz bandwidth is ∼30 dB-Hz for Ka-band. To

[3] S. Keihm, Jet Propulsion Laboratory, Pasadena, California, provided WVR data.

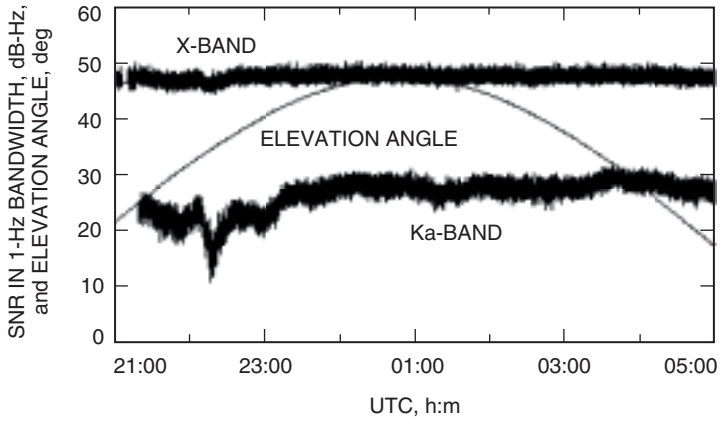

Fig. 5. MGS 1997/203-204 ETT P_c/N_o.

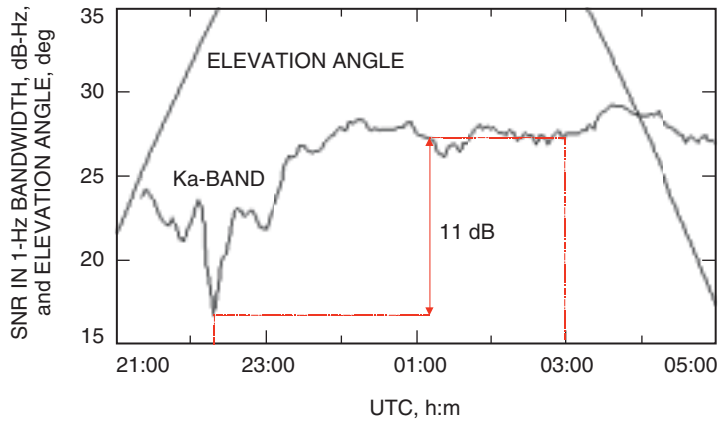

Fig. 6. MGS 1997/203-204 ETT Ka-band P_c/N_o (smoothed).

assess the effects of the deepest SNR fade feature at Ka-band ($P_c/N_o = 16.5$ dB near 203/22:18 UTC in Fig. 6), refer to the T_{op} plot of Fig. 1. Here the T_{op} reached a maximum value of $T_{op} = 320$ K at the time of the SNR fade feature, where the elevation angle was about 35 deg. A reference time at 204/03:00 UTC was chosen later in the pass during source set, which also was at an elevation angle of 35 deg, but when the weather was less severe. The T_{op} here was 130 K, and the Ka-band P_c/N_o was 27.5 dB-Hz. The air temperature was about 20 deg C, and the relative humidity was near 100 percent. The dB difference between these two data points is 11.0 dB. The effects on received SNR, P_c/N_o, due to weather will be a combination of added thermal noise (N_o) and atmospheric attenuation induced on the carrier signal power (P_c).

The dB difference contribution due to thermal noise (N_o) is estimated as

$$10\log\left(\frac{T_{op}(203/22{:}18\ \text{UTC})}{T_{op}(204/03{:}00\ \text{UTC})}\right) = 10\log\left(\frac{320}{130}\right) = 3.9\ \text{dB}$$

If all non-atmospheric contributions to the T_{op} ($\sim$76 K) are removed, the remaining temperature should be attributable to atmosphere alone. At 203/22:18 UTC, $T_{atm} = 320 - 76$ K $= 244$ K, and at 204/03:00 UTC, $T_{atm} = 130 - 76$ K $= 54$ K. For a consistency check at 204/03:00 UTC, the WVR 31.4-GHz zenith

temperature value of 36 K, scaled to the 35-deg elevation angle, is 56.5 K, consistent with the 54-K estimate from the TPR.

The atmospheric attenuation or loss factor (assuming a 280-K physical temperature for the atmosphere) is thus estimated as follows:

$$L_{atm} = 10\log\left(1 - \frac{T_{atm}}{T_{phys}}\right) = -8.9 \text{ dB at } 203/22{:}18 \text{ UTC}$$

$$= -0.9 \text{ dB at } 204/03{:}00 \text{ UTC}$$

A difference of 8.0 dB in attenuation due to atmosphere between the time tags is obtained. Together the thermal noise difference (3.9 dB) and attenuation difference (8.0 dB) between the two points results in about a 12-dB difference in P_c/N_o, which is in reasonable agreement with the 11-dB difference depicted in Fig. 6. The 1-dB difference between measured and estimated values was attained using simple differencing and does not take into account a more realistic atmosphere model (two-layer); nor have other effects, such as antenna wetting and temporal and spatial variations of the air physical temperature, been considered in this intended rough estimate.

The attenuation contribution (8.0 dB) therefore dominates over the thermal noise contribution (3.9 dB) to the overall degradation in P_c/N_o during the fade. The ETT, however, maintained lock throughout the entire period, as there was sufficient margin. The signature of the rain-fade event during the most severe of weather conditions is similar to those seen in Earth-orbiting satellite Ka-band data sets [6].

The corresponding X-band fade depth at 22:18 UTC is about 1-dB down relative to fade onset at 22:09 UTC, or 2-dB down relative to the nominal link P_c/N_o value of 48 dB-Hz. The 13.5-dB degradation from nominal for Ka-band and the 2-dB degradation from nominal for X-band are in agreement with independently computed attenuation values for similar wavelengths for very high rain rates [7].

C. Amplitude Fade Feature Analysis (Rain Fading)

The combined absorption and scattering on a radio wave passing through water droplets is the most significant propagation degradation, but its occurrence is sporadic, and it is a slow time-scale phenomenon (a time scale on the order of minutes). Figure 7 displays an expanded scale of the data in Fig. 6 for the Ka-band fade feature seen near 1997/203 22:18 UTC. In this case, the observed SNR was seen to decrease from 23 dB to 16.5 dB or about 6.5 dB over 9 min (540 s), resulting in a fade slope of about −0.7 dB/min or −0.012 dB/s. This fade slope estimate can be compared with the highest fade rate of −0.27 dB/s, measured by the Earth-orbiting Ka-band satellite community during a study of fade events at 19.44 GHz in E_b/N_o at the Boca Raton, Florida, site, which is subject to heavy rainfall. This fade depth may be characteristic of non-tropical sites for which similar dive and recovery features have been seen in the ACTS satellite data. The difference in these fade slopes (−0.012 dB/s for DSS 13 versus −0.27 dB/s for ACTS) can be reconciled with the conceptual picture of a weather front of a large rain cell moving across the antenna beam. A large front moving over the larger 34-m dish antenna at a given wind speed will have an averaging effect that should result in a gentler or less-steep slope and, hence, provide a bound on fade slope at the given wind speed. The range of fade durations or "spike" times for this magnitude of fade, inferred from WVR data, run about 400 to 3000 s depending on season and weather conditions.[4] The same front moving over the smaller ACTS Earth V-SAT antenna, 1.2 m in diameter, should result in a steeper slope in fade rate. If we scale the observed DSS-13 fade rate of −0.012 dB/s by the ratio of

[4] A. Mileant, personal communication, Jet Propulsion Laboratory, Pasadena, California, June 4, 2002, and "Telemetry Data Return Statistics vs. Zenith Noise Temperature," JPL Interoffice Memorandum 3315-01-02 (internal document), Jet Propulsion Laboratory, Pasadena, California, December 12, 2001.

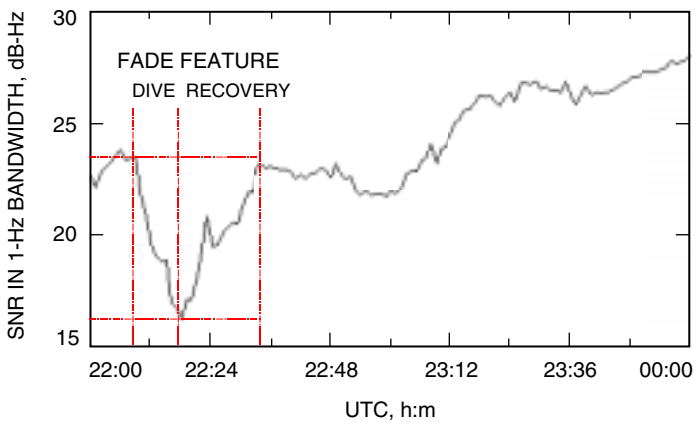

Fig. 7. MGS 1997/203-204 ETT Ka-band P_C/N_O (60-s average), close-up of fade feature at 22:18 UTC.

the diameters of the two antennas (34/1.2), the resulting scaled estimate of −0.34 dB/s for the predicted ACTS fade rate is comparable with the observed −0.27 dB/s. It is cautioned that this agreement may not always hold, especially in tropical climates where fade depths of similar magnitude may be significant at much shorter time scales.

The telemetry bit transmission rate usually will be much greater than the fluctuation or scintillation rates during severe weather conditions. The primary concern will be amplitude fading depth versus link margin. If the fade depth exceeds the link margin used, then the telemetry will be degraded. Thus, amplitude fade statistics are important to consider for a given tracking site and for setting the link margin and other parameters (see Subsection V.E).

D. Amplitude Autocorrelation Analysis (Scintillation)

Scintillation of a radio wave is characterized by rapid fluctuations (time scales on the order of seconds) in amplitude caused by fluctuations in phase, which in turn are caused by random variations in the refractive index of the irregularities as they cross the beam of the antenna. The magnitude of the scintillation phenomena (attributed to water vapor) is expected to be small compared to rain fading (attributed to liquid water or hydrometeors) for non-tropical climates and can be masked by thermal noise fluctuations.

Long-period elevation-angle-dependent trends due to changing gain of the antenna and system noise have not been removed from the signal strength data of Fig. 5. However, the atmospheric-induced effects appear to dominate over these long-period trends. Thus, neglecting these long-term trends, the focus is on short-period fluctuations. Given an antenna diameter of D and a wind speed of v_w, the length of time required for pockets of small cells of water vapor to cross the near-field antenna beam will be of the order D/v_w. Thus, most of the fluctuation energy due to these moving blobs is expected to correspond to time scales less than D/v_w.

To examine this supposition, the normalized autocorrelation function (see Fig. 8) was computed from the received Ka-band SNR data of Fig. 5 between 203/22:00 UTC and 204/05:00 UTC. The large spike at zero lag (thermal noise) and the "pedestal" spread of signal energy within 20 s of zero lag (scintillation) are prominent features in Fig. 8.

Figure 9 is a plot of the renormalized autocorrelation function of Fig. 8 after the contribution due to thermal noise at zero lag is removed. Also plotted in Fig. 9 is the exponential model curve using Eq. (4) with a value for τ_{HPHW} of 5 s, which nicely fit the data. This 5-s value for τ_{HPHW} corresponds to a

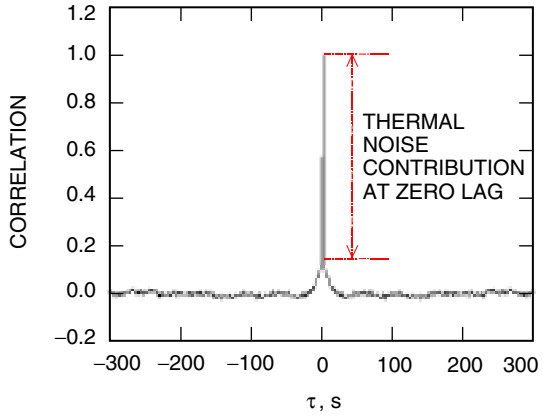

Fig. 8. 1997/203-204 Ka-band normalized autocorrelation function of SNR data of Fig. 3.

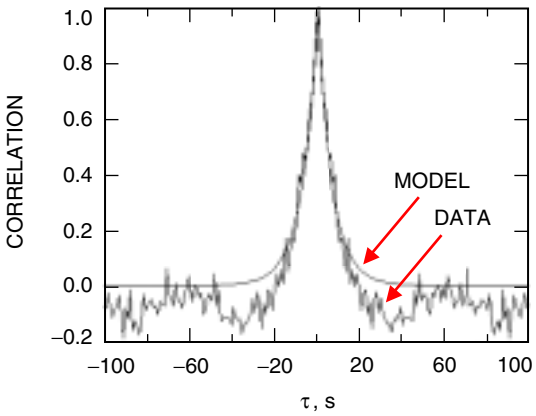

Fig. 9. 1997/203-204 Ka-band normalized autocorrelation function in Fig. 3 after thermal noise contribution at zero lag is removed, along with exponential model.

wind speed of 6.8 m/s over the 34-m diameter of the antenna, or 1.2 m/s over the estimated Fresnel-zone size of the irregularities. The actual average wind speed measured by ground sensors during this period was 3.3 m/s, which is reasonable considering that the spread of signal energy seen in the autocorrelation function is influenced by movement of irregularities all along the column of the antenna beam and not just at the ground. The wind speed also was changing during the experiment as well as, presumably, the size and number of the irregularities swept over the beam by the wind. Thus, short-period time scales provide a significant contribution to the overall fluctuation energy, as is evident upon inspecting the autocorrelation function (Fig. 9) within 5 s of zero lag. This feature is evidence of scintillation presumably caused by the troposphere. These short-term fluctuations in Ka-band signal strength do not significantly differ from those observed in adjacent fair-weather passes. In addition, these fluctuations are masked by thermal noise and are of significantly smaller magnitude than those of the observed rain fades.

E. Goldstone Fade Depth versus Telemetry Data Return

Curves of fade depth statistics versus percentage of the year that attenuation is exceeded are shown in Fig. 10. Here, the curves for the Earth-orbiting ACTS fade statistics at 27.5 GHz are presented for three selected sites;[5] they were originally published in [8]. Superimposed on Fig. 10 are 32-GHz curves [15] for the Deep Space Network tracking site at Goldstone, California.

The limited Goldstone curve implies a drier climate at Goldstone than at the ACTS sites. Differences in the curves between Goldstone and the ACTS sites could include complicating factors such as ACTS receive-terminal susceptibility to antenna and feed wetting. According to Crane [9], wet-antenna attenuation values as high as 7 dB beyond the atmospheric attenuation in the ACTS data could be due to the effect of water on the ACTS terminal reflector surfaces and feed windows.

Fades such as the 11-dB fade seen in the MGS 1997/203-204 pass occur less frequently, ∼0.01 percent of the time with an average duration on the order of 1000 s,[6] which is reasonably consistent with the observed 540-s fade duration. The absence of much shorter duration "deep" fades in the signal strength data during this worst-case rain-fade pass reinforces the expectation that the time scales of these rain fades, using a 34-m-diameter antenna, will be long compared to typical telemetry data rate periods.

[5] R. Acosta, NASA Glenn Research Center, Cleveland, Ohio, provided a CD of the summary of the NASA ACTS campaign, containing data sets, 2002.

[6] A. Mileant, personal communication, Jet Propulsion Laboratory, Pasadena, California, June 4, 2002.

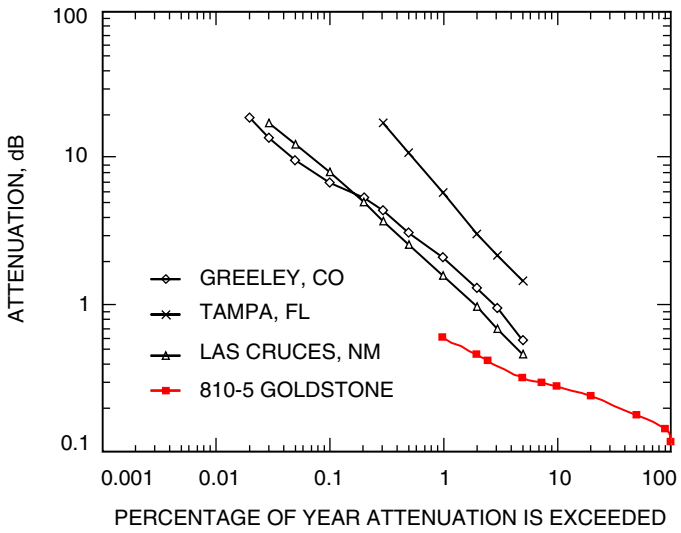

Fig. 10. Attenuation versus percent of year the value of attenuation is exceeded for ACTS 27.5-GHz propagation experiments ([10]) and Goldstone 32-GHz (from [15]).

F. Spacecraft Phase Data Analysis during Severe Weather

For MGS Ka-band pass 1997/203-204, the frequency data output from the ETT at 1-s intervals were processed using tools developed by the Radio Science Support Team. The model frequencies were computed using NAIF SPICE toolkit routines with an input SPICE kernel trajectory file supplied by the MGS Navigation Team. The troposphere model consisted of a simple zenith path delay and elevation-dependent ray-path model, which allowed the removal of a significant trend from the observed frequency data producing the frequency residuals shown in Figs. 11 and 12 for X-band and Ka-band, respectively. The path-delay effect on frequency, however, is due almost entirely to water vapor, whereas wet liquid dominates the long-period amplitude variations (see Fig. 5). The corresponding Allan deviations of the frequency residuals of Figs. 11 and 12 are shown in Figs. 13 and 14 for X-band and Ka-band, respectively.

Other examples of frequency residuals for less severe weather passes, such as 1997/205-206, are shown in Figs. 15 and 16 for X-band and Ka-band, respectively. The corresponding ASDs of these frequency residuals are shown in Figs. 17 and 18 for X-band and Ka-band, respectively. The frequency residuals and corresponding ASDs for other passes, such as one conducted on 1997/122, were similar.

The relative frequency fluctuation ASD curves, mapped from the Ka-band T_{op} fluctuation ASD (such as shown in Fig. 2), using Eqs. (2) and (3), and the ASD of the actual ETT Ka-band frequency residuals (such as shown in Figs. 12 and 16) are displayed in Fig. 19(a) for pass 1997/203-204, Fig. 19(b) for pass 1997/205-206, and Fig. 19(c) for pass 1997/122. Also shown in these figures are dashed lines of model approximations of the form $\sigma_y(\tau) \sim \tau^{-\alpha}$, using particular values of the power-law slope, α.

The major conclusion for pass 1997/203-204, upon inspection of Fig. 19(a), is that the predicted ASD curve lies an order of magnitude higher than the measured ASD curve, implying that the T_{op} fluctuations are dominated by liquid water. The measured values of ASD of the signal phase (in the form of frequency residuals) are sensitive only to water vapor and are not significantly influenced by the liquid water.

On the other hand, the predicted ASD curves for the fair-weather passes are in agreement with the measured frequency ASD curves for pass 1997/205-206 [see Fig. 19(b)] and for pass 1997/122 [see Fig. 19(c)]. This suggests that temperature fluctuations are dominated by water vapor during

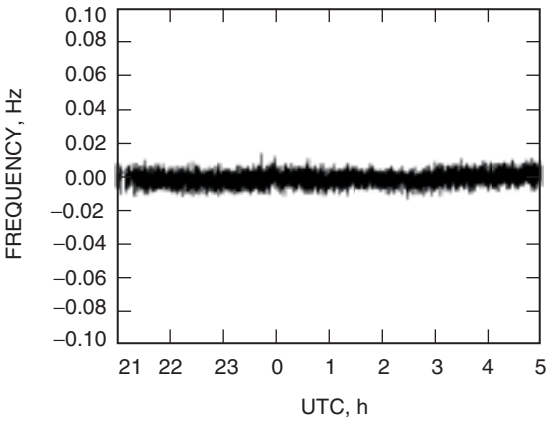

Fig. 11. 1997/203-204 X-band frequency residuals.

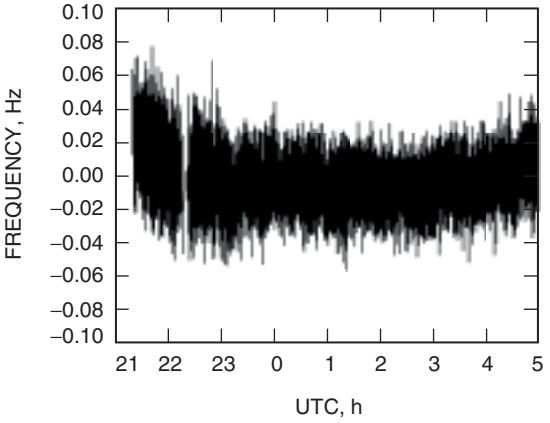

Fig. 12. 1997/203-204 Ka-band frequency residuals.

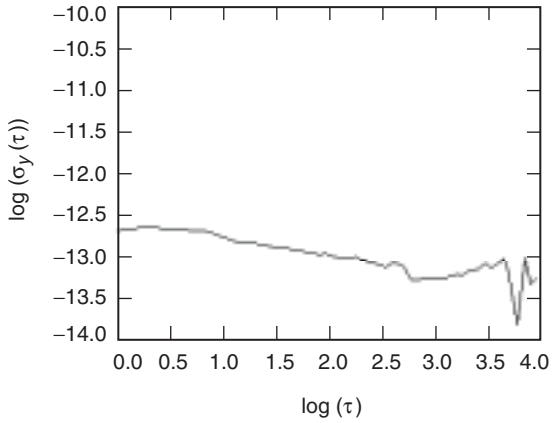

Fig. 13. 1997/203-204 log (Allan deviation) of X-band frequency residuals.

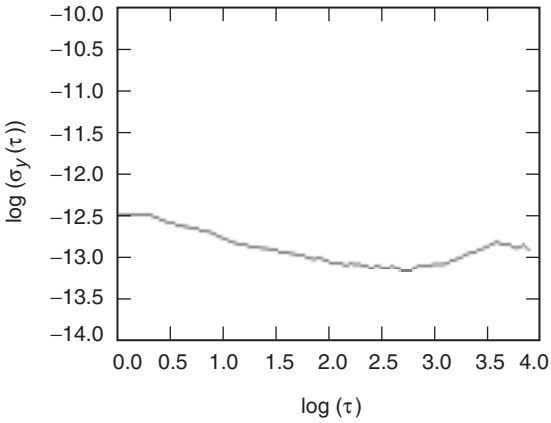

Fig. 14. 1997/203-204 log (Allan deviation) of Ka-band frequency residuals.

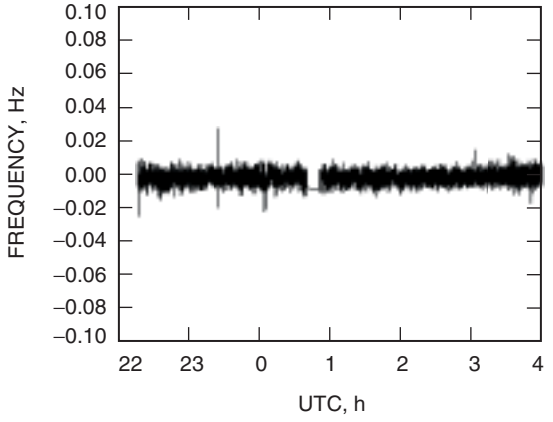

Fig. 15. 1997/205-206 X-band frequency residuals.

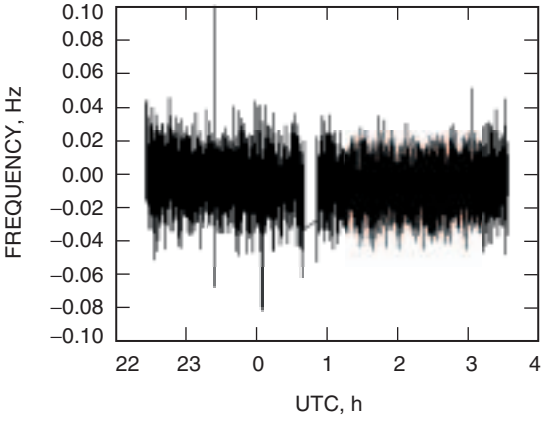

Fig. 16. 1997/205-206 Ka-band frequency residuals.

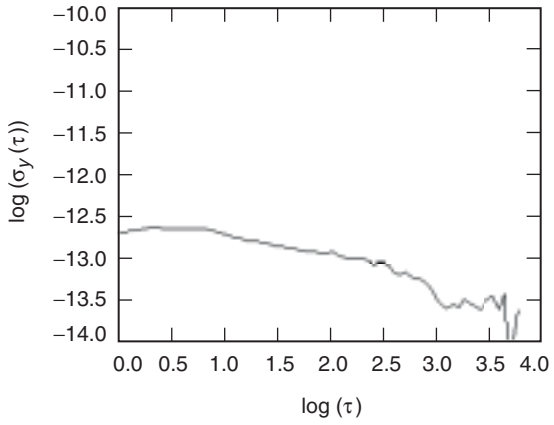

Fig. 17. 1997/205-206 log (Allan deviation) of X-band frequency residuals.

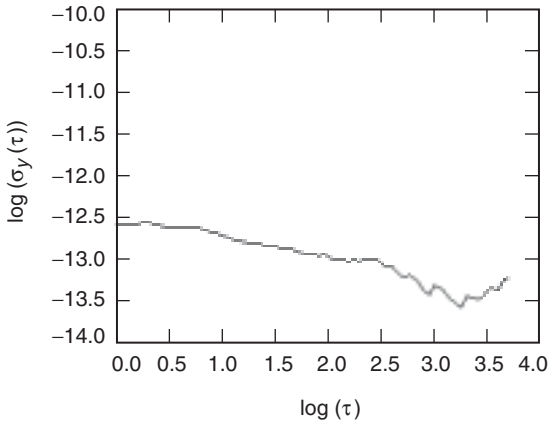

Fig. 18. 1997/205-206 log (Allan deviation) of Ka-band frequency residuals.

less severe weather, as very little liquid water is present in the atmosphere. The conversion of the Ka-band temperature fluctuations to Ka-band phase fluctuations for fair-weather passes, 97/122 and 97/205-206, in the form of predicted ASDs is shown in Fig. 20 along with that of severe-weather pass 1997/203-204.

The driest weather pass (1997/122) measured frequency ASD curve lies further below the ASD curves of passes 1997/205-206 and 1997/203-204, consistent with the drier conditions, and agrees well with its predicted ASD curve derived from the system temperature fluctuations.

The power-law slope, α, of the measured ASD curves tends to be about 0.25 for short time scales and about 0.45 for longer time scales for the driest weather pass, 1997/122 [Fig. 19(c)]. However, the power-law slope fit from the measured frequency ASD curves for passes 1997/203-204 and 1997/205-206 is $\sim$0.3 for time scales below 1000 s, while for the predicted ASD, a slope of 0.45 appears to fit better [Figs. 19(a) and 19(b)]. These power-law slopes are consistent with the model approximation ($\sigma_y(\tau) = c\tau^{-\alpha}$) power-law exponents expected due to troposphere, which range from $\alpha = 1/6$ for short time scales to $\alpha = 2/3$ for long time scales [10]. These measured values of power-law index also are consistent with measurements obtained from ASDs of very long baseline interferometry (VLBI) phase fluctuations, $\alpha = 0.25$ to 0.50, which were attributed to wet troposphere [11]. The values of α fit to the predicted frequency ASD curves at the longer time intervals, $\alpha = 0.45$ for 1997/203-204 [Fig. 19(a)], are consistent with the range of exponents expected based on models and previous measurements [10].

The Ka-band measured frequency ASD curves appear to be limited by troposphere for all three passes, as judged by the slopes of the ASD signature, which are consistent with values expected for the troposphere. ASD curves of the ionosphere contribution to the downlink X-band phase also were estimated using difference X-/Ka-band frequency residuals ($f_X - f_{Ka}/3.8$). This ASD curve thus should approximate the charged-particle contribution of the uplink X-band phase, which would be a contributor on the Ka-band downlink signal phase. This curve lies significantly below the measured Ka-band frequency residual ASD curve, providing an additional degree of confidence that the troposphere, not the ionosphere, dominates the Ka-band downlink signal phase.

Even for the severe-weather pass 1997/203-204, the measured frequency ASD curve [Fig. 19(a)] does not appear to differ significantly from the frequency ASD curves of the fair-weather passes [Figs. 19(b) and 19(c)]. For 1997/205-206 and 1997/122, the predicted ASD from temperature fluctuations and measured ASD from signal phase are in agreement, suggesting that water vapor dominates the temperature fluctuations. For pass 1997/203-204, the significantly elevated temperature-induced predicted ASD curve lies above the ASD curve measured from signal phase, implying significant water liquid sensed by the

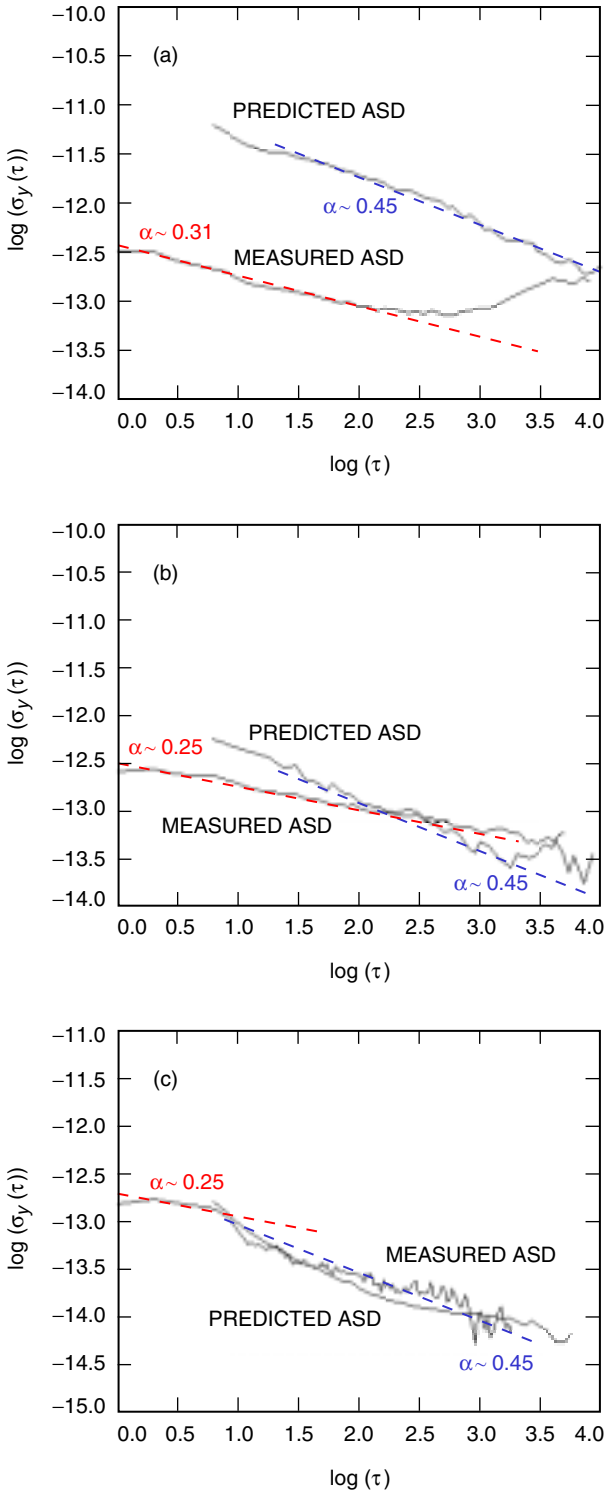

Fig. 19. Ka-band predicted ASD of relative frequency fluctuations and actual frequency ASD: (a) 1997/203-204, (b) 1997/205-206, and (c) 1997-122.

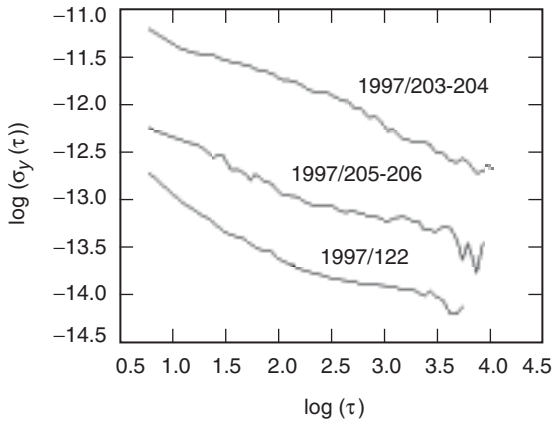

Fig. 20. Ka-band predicted ASD of relative frequency fluctuations mapped from TPR fluctuations.

temperature data but not by signal phase data. Given that the fluctuations seen in the X-band and Ka-band TPR data are correlated and of the appropriate relative expected proportions due to troposphere, and that the estimated thermal noise and ionosphere contributions lie below the measured and predicted frequency ASD curves, there is a high degree of confidence that the fluctuations seen in the measured frequency ASDs are attributable to troposphere.

The slopes of the measured frequency residual ASD curves versus time scale in Figs. 19(a) through 19(c) do not overtly turn over to take on positive values (negative α), which is expected at very short time scales due to beam averaging [12]. Upon close inspection of these curves, there is evidence of flattening at the very short time scales, and even a hint of turnover. The crossover time expected for such a turnover occurs between 1 and 5 s [12]. The assumption that the wind speed is constant over all heights in the atmospheric column above the antenna may not be true during this time. Hence, there may be a weak correlation with wind speed, and thus the slope may flatten out instead of turning down. The observed trend is consistent with the hypothesis that the effect of the wind speed over the aperture is being averaged over column height.

The dominant effect of severe weather on received spacecraft signals will be deep amplitude fades with relatively long time durations. Signal phase will be significantly less affected. The optimal tracking-loop bandwidth setting of a receiver during severe weather appears to be nominal, and would need to account for only the increased thermal noise resulting from the hydrometeors.

VI. Discussion

In the previous study [1], the atmospheric contribution to the X-band and Ka-band total T_{op} for passes conducted during the latter half of 2001 was examined. The ratio of the Ka-band to X-band atmospheric noise temperature contribution to the T_{op} was examined for both clear and severe weather conditions. For relatively clear weather conditions, this ratio was normally about four, which is expected since the ratio for oxygen only is about 3.5. During cloudy or rainy weather conditions, this ratio reached values of 6 or higher, which is expected since this ratio, due to water vapor only, will reach values of about 13. During rainy weather, this ratio is expected to be higher.

For the MGS severe-weather pass 1997/203-204, the subject of this study, a similar approach was employed, which allowed T_{atm}, the individual atmospheric contributions to T_{op}, to be computed and plotted for both X-band and Ka-band, as displayed in Fig. 3.

The ratio of Ka-band to X-band atmosphere contribution to the T_{op} after correcting to zenith is shown in Fig. 4 for 1997/203-204. This ratio significantly exceeds 13 during the feature observed between 22:30 and 23:30 UTC. Given that the antenna was pointing into a dense rain cell near the horizon during this time, such high ratios may be the result of effects that become significant as the droplet size becomes comparable to wavelength. The absorption contribution increases as the droplet starts to behave like a resonator. Another factor may be that water collects in the holes of the antenna panels and there may be leakage through the dish surface;[7] that is, significantly more ground noise at Ka-band is picked up when the antenna surface is wet. Because the feed packages are located in the isolated pedestal room, presumably water has not collected on the feed package Kapton covers.

Using results derived from Gunn and East [7], a ratio for similar wavelengths (0.9 cm and 3 cm) was found to reach values of about 20 due to scattering or attenuation by rain for high rain rates of 100 mm/h. The observed peak value of this ratio in Fig. 4 appears to be consistent with rain-induced effects.

At wavelengths shorter than 10 cm, the attenuation through rain depends explicitly on the diameter of the droplets as well as the water content [7]. For a rainfall rate of 150 mm/h, the attenuation at Ka-band can reach values of 30 dB/km, while for X-band the attenuation is about 6 dB/km. For experiment 1997/203-204, the largest X-band SNR fade (from nominal) was about 2 dB, while for Ka-band it was about 13.5 dB (from nominal) (see Subsection V.B).

Although there is an expected scaling error since the weather model used input surface meteorological data to calibrate out the baseline troposphere, the significant short-term fluctuation peaks in Fig. 4 are attributed to liquid water in clouds traversing the antenna beam. Ka-band is expected to be more susceptible to effects of liquid water than is X-band. It should be kept in mind that the Ka-band noise temperature also is more susceptible to water vapor than is X-band, although the change in path delay may be roughly the same at both frequencies.

For reference, the atmospheric temperature contribution extracted from the T_{op} data for the fair-weather pass 1997/205-206 is shown in Fig. 21 for X-band and Ka-band, and the corresponding Ka-band-to-X-band atmospheric temperature ratio—about 3.5, consistent with dry weather—is shown in Fig. 22. A small, non-weather feature is apparent in the X-band data at ∼206/00:30 UTC. For pass 1998/090-091, the atmospheric temperature is shown in Fig. 23 (with a conspicuous weather-related feature visible from 091/00:30 to 091/01:00 UTC), and the corresponding ratio between frequency bands is shown in Fig. 24.

During the rainy weather pass 1997/203/204, both rain-fade (Subsection V.C) and scintillation (Subsection V.D) were detected in the received signal-strength (or amplitude) data output from the ETT. A rain-fade event can be characterized by a large rain cell moving over the antenna beam at a specific wind velocity. The time scale of the fade will be on the order of the cell size divided by the wind speed and tends to be of several-minutes duration. A scintillation event is due to the fluctuations or variations of water-droplet or vapor irregularities, whose sizes are of the order of a Fresnel zone as they are carried over the antenna beam by the wind. The time scales for diffraction are of the order of the Fresnel-zone size divided by the wind speed and tend to have durations of several seconds.

VII. Spacecraft Telemetry Considerations

The TPR zenith sky temperature data presented in the first article [1] at 1-s time scales have fluctuations that are dominated by system noise (gain instability and thermal) during clear-weather passes and by the wet troposphere for cloudy/rainy weather passes. The effect of increased cloudy or rainy weather will be increased fluctuations on T_{op} measurements and increased attenuation on received spacecraft signals.

[7] R. Clauss, personal communication, Jet Propulsion Laboratory, Pasadena, California, 2002.

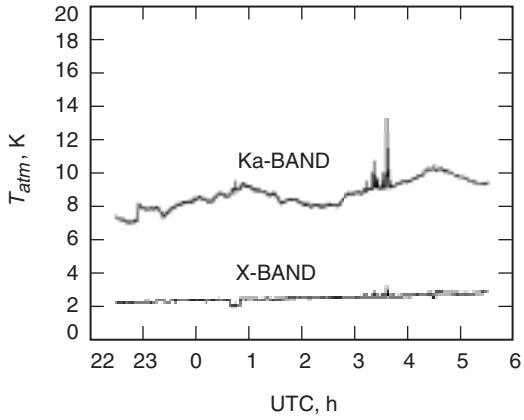

Fig. 21. 1997/205-206 T_{atm}.

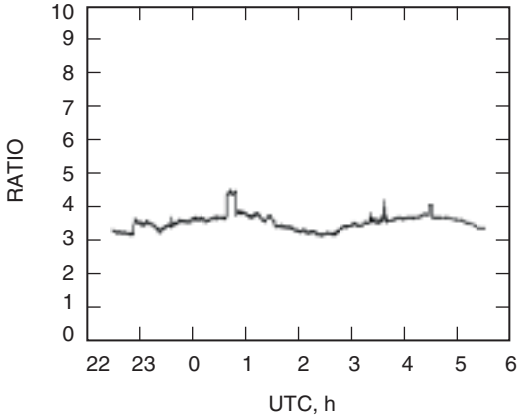

Fig. 22. 1997/205-206 ratio of T_{atm} (Ka)/T_{atm} (X).

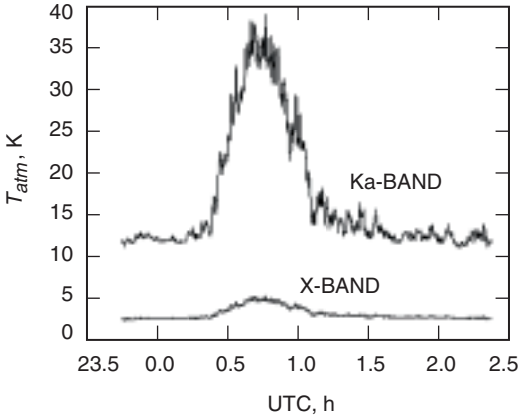

Fig. 23. 1998/090-091 T_{atm}.

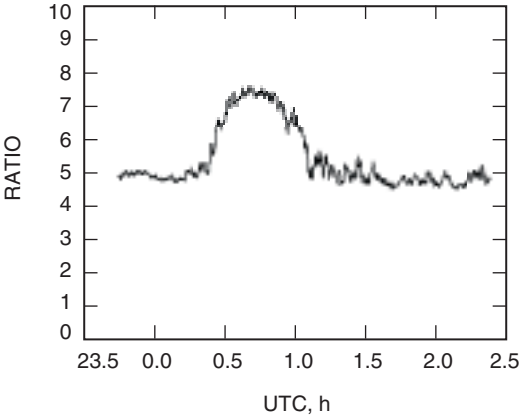

Fig. 24. 1998/090-091 ratio of T_{atm} (Ka)/T_{atm} (X).

All indications from the experience of Earth-orbiting satellite Ka-band operations are that, if there is sufficient margin, telemetry data can be reliably acquired, even at very high data rates.[8] However, if a fade falls below a threshold, the data will be degraded.

The measured phase (or frequency) ASD appears to be sensitive only to water vapor, while the predicted ASD derived from the fractional temperature fluctuations includes significant contributions due to liquid water when the weather is rainy. The extrapolation of the frequency ASD to short time scales is expected to fall below the thermal noise floor and, thus, ceases to be a concern. The tracking-loop bandwidth setting of a receiver during severe-weather passes appears to be nominal and only would need to account for any increased thermal noise. However, the phase residual ASD during fair-weather passes appears to agree with the predicted ASD from the temperature fluctuations, suggesting that the temperature fluctuations are dominated by water vapor for the 1-s to 1000-s time scales.

The dominant effect of cloudy/rainy weather on received spacecraft signals will be deep amplitude fades but with reasonably long time durations. Signal phase will be significantly less affected. Site-dependent attenuation statistics are important for setting parameters in Ka-band telemetry data acquisition operations.

[8] R. Acosta, personal communication, NASA Glenn Research Center, Cleveland, Ohio, 2002.

Future work involves conducting experiments and performing analysis to assess the effects of the troposphere on Ka-band spacecraft telemetry at short time scales, which are comparable to the frame periods utilized. Such efforts would include simulations, experiments using real spacecraft telemetry, theoretical analysis, and additional TPR experiments at Ka-band using much shorter integration times (<1 s). Shambayati [14] discusses strategies for maximizing data return at X-band and Ka-band. Plans for mitigating weather and other effects for DSN Ka-band operations are presented by Pham and Townes [13]. The upcoming Mars Reconnaissance Orbiter (MRO) will have an active Ka-band communications link, for which several demonstrations are being planned.

Acknowledgments

I would like to thank R. Clauss, R. Hastrup, C. Naudet, L. Paal, S. Keihm, A. Tanner, and S. Shambayati for their comments, informative discussions, and suggestions; the DSS-13 station personnel for their assistance in acquiring the data; R. Ceserone, R. Hastrup, L. Paal, and J. Wyatt for their support of this work; S. Asmar and the Radio Science Support Team for providing support, especially D. Johnston for software support in the processing of the frequency data acquired from the experiments; S. Keihm for providing WVR data used in the analysis; and R. Acosta at NASA Glenn Research Center for providing information on ACTS satellite data results. Finally, I would like to acknowledge Nasser Golshan for the many motivating discussions that I had with him over the last few years on the subject of Ka-band signal propagation. Nasser, who tragically passed away on June 5, 2002, had the vision to realize the importance and operational significance of understanding signal variations at Ka-band, and this played a noteworthy role in the initiation of this study.

References

[1] D. D. Morabito, "Ka-band Atmospheric-Induced Temperature Fluctuations," *The Interplanetary Network Progress Report 42-150, April–June 2002,* Jet Propulsion Laboratory, Pasadena, California, pp. 1–17, August 15, 2002. http://ipnpr.jpl.nasa.gov/progress_report/42-150/150D.pdf

[2] S. Johnson, R. Acosta, and W. Gauntner, "Impact of Various Fade Mitigation Techniques Using Data from the ACTS Propagation Campaign," AIAA 19th International Communications Satellite Systems Conference, Toulouse, France, April 2001.

[3] R. Crane and D. Rogers, "Review of the Advanced Communications Technology Satellite (ACTS) Propagation Campaign in North America," *IEEE Antenna and Propagation Magazine,* vol. 40, no. 6, pp. 23–28, December 1998.

[4] D. Morabito, S. Butman, and S. Shambayati, "The Mars Global Surveyor Ka-band Link Experiment (MGS/KaBLE-II)," *The Telecommunications and Mission Operations Progress Report 42-137, January–March 1999,* Jet Propulsion Laboratory, Pasadena, California, pp. 1–41, May 15, 1999. http://tmo.jpl.nasa.gov/progress_report/42-137/137D.pdf

[5] R. Vessot, "Frequency and Time Standards," *Methods of Experimental Physics,* vol. 12, part C, *Astrophysics, Radio Observations,* edited by M. Meeks, New York: Academic Press, pp. 198–227, 1976.

[6] C. Cox and T. Coney, "Advanced Communications Technology Satellite (ACTS) Fade Compensation Protocol Impact on Very Small-Aperture Terminal Bit Error Rate Performance," *IEEE Journal on Selected Areas in Communications,* vol. 17, no. 2, pp. 173–179, February 1999.

[7] K. L. S. Gunn and T. W. R. East, "The Microwave Properties of Precipitation Particles," *Quart. J. Roy. Meteorol. Soc.,* vol. 80, pp. 522–545, October–December 1954.

[8] D. Rogers and R. Crane, "Review of Propagation Results from the Advanced Communications Technology Satellite (ACTS) and Related Studies," *IEEE Trans. Commun.,* vol. E84-B, no. 9, pp. 2357–2368, September 2001.

[9] R. K. Crane, "Analysis of the Effects of Water on the ACTS Propagation Terminal Antenna," *IEEE Transactions on Antennas and Propagation,* vol. 50, no. 7, pp. 954–965, July 2002.

[10] R. Treuhaft and G. Lanyi, "The Effect of the Dynamic Wet Troposphere on Radio Interferometric Measurements," *Radio Science,* vol. 22, no. 2, pp. 251–265, March–April 1987.

[11] A. Rogers, A. Moffet, D. Backer, and J. Moran, "Coherence Limits in VLBI Observations at 3-Millimeter Wavelength," *Radio Science,* vol. 19, pp. 1552–1560, 1984.

[12] R. Linfield, "The Effect of Aperture Averaging Upon Tropospheric Delay Fluctuations Seen With a DSN Antenna," *The Telecommunications and Data Acquisition Progress Report 42-124, October–December 1995,* Jet Propulsion Laboratory, Pasadena, California, pp. 1–7, February 15, 1996.
http://tmo.jpl.nasa.gov/progress_report/42-124/124A.pdf

[13] T. Pham and S. Townes, "Migration Plan Toward Ka-band Operations in the Deep Space Network," AIAA paper 2002-2068, 20th AIAA International Communications Satellite Systems Conference and Exhibit, Montreal, Quebec, May 12–15, 2002.

[14] S. Shambayati, "Maximization of Data Return at X-band and Ka-Band on the DSN's 34-Meter Beam-Waveguide Antennas," *The Interplanetary Network Progress Report 42-148, October–December 2001,* Jet Propulsion Laboratory, Pasadena, California, pp. 1–20, February 15, 2002.
http://ipnpr.jpl.nasa.gov/progress_report/42-148/148E.pdf

[15] *DSMS Telecommunications Link Design Handbook,* TMOD 810-005, Rev. E, JPL D-19379, Rev. E., Module 105, Jet Propulsion Laboratory, Pasadena, California, January 15, 2001.